Interlaminar Stress Recovery for Three-Dimensional Finite Elements

C. Fagiano, M.M. Abdalla, C. Kassapoglou, Z. Gürdal

Interlaminar Stress Recovery for Three-Dimensional Finite Elements

C. Fagiano, M.M. Abdalla, C. Kassapoglou, Z. Gürdal

PII: S0266-3538(09)00438-2
DOI: 10.1016/j.compscitech.2009.12.013
Reference: CSTE 4593

To appear in: *Composites Science and Technology*

Received Date: 17 November 2009
Revised Date: 7 December 2009
Accepted Date: 13 December 2009

Please cite this article as: Fagiano, C., Abdalla, M.M., Kassapoglou, C., Gürdal, Z., Interlaminar Stress Recovery for Three-Dimensional Finite Elements, *Composites Science and Technology* (2009), doi: 10.1016/j.compscitech.2009.12.013

Interlaminar Stress Recovery for Three-Dimensional Finite Elements

C. Fagiano*,a,1, M. M. Abdalla[a], C. Kassapoglou[a], Z. Gürdal[a]

[a] *Faculty of Aerospace Engineering, Delft University of Technology, Kluyverweg 1, 2629 HS Delft, The Netherlands*

Abstract

An accurate evaluation of interlaminar stresses in multilayer composite laminates is crucial for the correct prediction of the onset of delamination. In general, three dimensional finite element models are required for acceptable accuracy, especially near free edges and stress concentrations. Interlaminar stresses are continuous both across and along layer interfaces. Nonetheless, the continuity of interlaminar stresses is difficult to enforce in C^0 interpolated elements. Nodal values of the stresses are usually retrieved using extrapolation techniques from super-convergent points, if known, or Gauss points inside the element. Stress fields within an element can be deduced using either constitutive relations or variationally consistent procedures. In either case, spurious oscillations in stress fields may be encountered leading to a reduced accuracy of the recovered stresses at nodes. In this paper, an efficient interlaminar stress recovery procedure for three-dimensional finite element formulations is presented. The proposed procedure does not rely on extrapolation techniques from super-convergent or integration points. Interlaminar stress values are retrieved directly at nodes and stress continuity at the inter-element boundary is automatically satisfied. Several benchmark problems were analysed. Comparisons with finite element software and available solutions in the literature confirmed the accuracy of the procedure. Accurate interlaminar stresses were obtained using coarser meshes compared to customary recovery procedures.

Key words: A. Layered structures, B. Mechanical properties, C. FEA, Interlaminar stresses.

*Corresponding author

Email address: c.fagiano@tudelft.nl, Telephone: +31.15.27.85386, Fax: +31.15.27.85337 (C. Fagiano)

[1] PhD Student.

1. Introduction

An accurate evaluation of interlaminar stresses in multilayer composite laminates is crucial for the correct prediction of delamination initiation. Due to its importance, this subject has been the focus of numerous researchers. Several levels of modelling can be used for the evaluation of interlaminar stresses. The simplest approach is based on using Classical Laminated Plate Theory (CLPT). While, CLPT assumes a state of plane stress within each lamina of a multi-directional laminate, interlaminar stresses are most commonly obtained by integrating the three-dimensional equilibrium equations of elasticity through the thickness [1, 2]. Nonetheless, three dimensional stress states cannot, in general, be accurately analysed, and three dimensional theories are required for acceptable accuracy. This is especially true in regions such as free edges and regions of stress concentration where the basic assumptions of CLPT are no longer valid. Transverse shear stresses are directly accounted for in the First Order Shear Deformation Plate Theory and higher order theories [2, 3]. These Equivalent Single Layer (ESL) theories have limited accuracy in predicting interlaminar stresses because of their failure to account for both Zig-Zag effects (rapid change of slope across layer interfaces due to through the thickness discontinuity of mechanical properties) of the displacement fields in the thickness direction and interlaminar continuity of the transverse stress field [4]. Thus, for accurate evaluation of interlaminar stresses, three-dimensional elasticity is the tool of choice. This is reflected in the profusion of layerwise (LW) theories [3, 4, 5] and efficient solid shell elements [2, 4].

Within the class of three-dimensional elements, an important issue is the accurate calculations of stresses. Stress recovery is highly dependent on the design of the particular element and on the formulation used in deriving the element. Mixed formulations provide more flexibility in the construction of efficient elements compared to classical formulations. Although primarily motivated by avoidance of the locking phenomena in finite element solutions, mixed formulations based on the Reissner or Hu-Washizu functional [6, 7], with displacements, stresses and/or strains as field variables, are so closely related to stress recovery that the formulations can also be viewed as stress recovery methods [8]. Mixed Layer-Wise theories are exemplified by the work of Carrera [9], where a Reissner's mixed variational equation [10, 11] is used to derive the governing equations in terms

of displacements and transverse stress variables [12, 13]. On the one hand assumed stress methods do not require any post-processing for the accurate recovery of stresses. On the other hand, inverse constitutive relations which define strains in terms of stress measures are employed greatly complicating the extension to the nonlinear case. Another shortcoming is the great added burden of solving simultaneously for stress and displacement degrees of freedom.

A particular form of the three field Hu-Washizu variational principle has been presented by Simo and Rifai [14], who developed a class of assumed mixed finite element methods to allow the systematic development of low order elements possessing good coarse mesh and distortion insensitive properties. The strain approximation is split into two parts: one is the usual displacement-gradient term, and the second is an enhanced strain part. Of particular note is the solid shell element developed by Vu-Quoc and Tan [15, 16]. For these three-dimensional enhanced strain elements, C^0 interpolated displacement fields are used. Physically, interlaminar stresses are continuous both across and along layer interfaces. Nonetheless, the continuity of interlaminar stresses is difficult to enforce in C^0 interpolated elements. Stress recovery procedures are necessary to find acceptably accurate stress fields.

Many researches have focussed on developing reliable stress recovery procedures. Early attempts to construct effective procedures included: the interpolation-extrapolation from super-convergent points [17], the L_2 projection [18], the stress smoothing [19, 20], and the integral stress technique [21]. Zienkiewicz and Zhu [22, 23] made a very significant breakthrough towards an efficient post-processing technique when they proposed the super-convergent patch recovery (SPR) procedure. Many investigators have modified this procedure to include satisfaction of boundary conditions [24, 25, 26]. For a more accurate prediction of the transverse stresses in laminated composites and shells, a Modified Super-convergent Patch Recovery (MSPR) technique has been derived to obtain accurate nodal in-plane stresses which, subsequently, are used in the integration along the thickness of the equilibrium equations for evaluating the transverse shear and normal stresses [27]. Patch recovery procedures depend crucially on the accurate evaluation of stresses within elements. Stress fields within an element can be deduced using either constitutive relations or variationally consistent procedures. Stress fields deduced using constitutive relations can show spurious

oscillations due to the retention of higher order (inconsistent) terms which do not contribute to the determination of the displacements and strains, which then get reflected as extraneous stress oscillations [28, 29]. As far as variationally consistent procedures are concerned, it is worth mentioning the weighted residual approach developed by De Miranda and Ubertini [30]. Nevertheless, even variationally consistent procedure suffer from spurious oscillations in stress fields as shown by Dakshina-Moorthy and Reddy [31].

The purpose of this paper is to present an efficient interlaminar stress recovery procedure within three dimensional FE formulations that is able to overcome the problems usually encountered using customary procedures, i.e. severe oscillations of stress distributions, without relying on extrapolation techniques from super-convergent points. Thus, the accuracy of the recovered interlaminar stresses is not dependent on the knowledge of superconvergent point nor is it sensitive to the stress recover method employed to obtain element stress distributions. Moreover, the procedure attains as much accuracy as assumed stress methods using coarser meshes and without the need to include stress degrees of freedoms in the solution process. The proposed procedure was developed based on equilibrium considerations, and interlaminar stresses are recovered directly at nodes. The numerical formulation is presented and explained in detail in the next section. The reliability of the approach is tested analysing several benchmark problems, and the results are reported in section 3. Conclusions and future developments are addressed in section 4.

2. Interlaminar stresses recovery procedure

The present procedure is an extension of the interlaminar stress recovery procedure developed by Dakshina Moorthy and Reddy [31] in the context of studying delamination in multilayered composites. In their approach, each ply is modelled as a separate body and the interlaminar boundary is treated as a contact surface. The interlaminar forces are obtained using an interface model based on the penalty method. Using these contact loads the interlaminar stresses are recovered.

The recovery procedure partitions the contact surface into a set of non-overlapping patches corresponding to groups of elements. The traction distribution is interpolated over each patch in terms of nodal values. Static equivalence between the tractions and the contact forces is used to calcu-

late the nodal value of the tractions, hence the interlaminar stresses. The procedure was found in practice to lead to oscillatory interlaminar stresses. Thus, a final step is the application of a smoothing technique to obtain more physically meaningful interlaminar stresses.

The present procedure extends the procedure of Dakshina Moorthy and Reddy in two ways. First, each ply is still modelled separately but the compatibility between the plies is enforced using Lagrange multipliers following the procedure commonly employed in domain decomposition methods. Thus, connecting forces are obtained without resorting to a penalty formulation. Second, the traction distribution is interpolated over the complete interlaminar surface. Thus, the full distribution of interlaminar stresses is obtained simultaneously. In the following, we give more details about the proposed formulation.

Consider a typical interface between two plies as shown in figure 1. The system of linear equilibrium equations and compatibility conditions can be written as,

$$\begin{bmatrix} \boldsymbol{K}^{(1)} & 0 & \boldsymbol{B}^{(1)^T} \\ 0 & \boldsymbol{K}^{(2)} & \boldsymbol{B}^{(2)^T} \\ \boldsymbol{B}^{(1)} & \boldsymbol{B}^{(2)} & 0 \end{bmatrix} \begin{bmatrix} \boldsymbol{u}^{(1)} \\ \boldsymbol{u}^{(2)} \\ \boldsymbol{\lambda} \end{bmatrix} = \begin{bmatrix} \boldsymbol{f}^{(1)} \\ \boldsymbol{f}^{(2)} \\ 0 \end{bmatrix} \tag{1}$$

where $\boldsymbol{K}^{(1)}$ and $\boldsymbol{K}^{(2)}$ are the stiffness matrices of the two plies, $\boldsymbol{u}^{(1)}$ and $\boldsymbol{u}^{(2)}$ the displacement vectors of the two plies, $\boldsymbol{f}^{(1)}$ and $\boldsymbol{f}^{(2)}$ the load vectors of the two plies, $\boldsymbol{B}^{(1)}$ and $\boldsymbol{B}^{(2)}$ are the Boolean matrices providing the equality conditions between displacements of the two plies, and $\boldsymbol{\lambda}$ are the Lagrange multipliers (interlaminar forces) introduced to enforce the compatibility constraints between the plies. Solving the system of equations (1), the interlaminar forces between the plies are obtained as well as displacements.

The traction distribution $\boldsymbol{t}$ over a surface element is interpolated using C^0 iso-parametric shape functions,

$$\boldsymbol{t} = \boldsymbol{N}\,\boldsymbol{t}_f \tag{2}$$

where $\boldsymbol{t}_f$ is the vector of the nodal traction values and $\boldsymbol{N}$ is the matrix of C^0 shape functions. The surface element connectivity is directly inherited from the solid element faces.

Displacements over a surface element are interpolating using the same C^0 iso-parametric shape

functions. Thus, the internal work W_{in} done by the tractions over the element surface can be written as,

$$W_{in} = \int_{\Omega_f} \underbrace{(\boldsymbol{t}_f \boldsymbol{N})^T}_{\text{traction}} \underbrace{\boldsymbol{N}\,\partial \boldsymbol{q}_f}_{\text{disp.}}\, \partial\Omega_f = \boldsymbol{t}_f^T \boldsymbol{M}_f\, \delta \boldsymbol{q}_f. \tag{3}$$

where $\boldsymbol{q}_f$ is the vector of nodal displacements, and $\boldsymbol{M}_f$ is the matrix of areas,

$$\boldsymbol{M}_f = \int_{\Omega_f} \boldsymbol{N}^T \boldsymbol{N}\, \partial\Omega_f. \tag{4}$$

The surface element contributions are assembled over the complete interlaminar surface in a matrix $\boldsymbol{M}$, and considering the static equivalence between the tractions and the connecting forces, the following relation is obtained,

$$\boldsymbol{M}\,\boldsymbol{t} = \boldsymbol{\lambda} \tag{5}$$

where $\boldsymbol{t}$ is the global vector of nodal traction. The process is repeated for every interlaminar surface of interest. The accuracy of the present approach is demonstrated in the next section.

3. Numerical Results

3.1. Simply supported plate subjected to bisinusoidal pressure load

The present procedure was validated considering a benchmark problem analysed by Pagano [32], where three dimensional exact elasticity solutions of idealised simply supported cross-ply [0°/90°/0°], square plates under bisinusoidally distributed pressure load of intensity p_z, are provided. The length and thickness of the plate is denoted by "a"and "H"respectively. The laminate is made of material plies that are idealized to be homogeneous, elastic and orthotropic. The following material properties are used: $E_{11} = 25\,GPa$, $E_{22} = E_{33} = 1\,GPa$, $G_{12} = G_{13} = 0.5\,GPa$, $G_{23} = 0.2\,GPa$, and $\nu_{12} = \nu_{13} = \nu_{23} = 0.25$. Subscripts 1,2 and 3 denote the fibre, transverse and thickness directions, respectively. The rectangular Cartesian coordinate system used is such that the origin is located at the center of the middle layer of the plate. Stresses are normalized

according to the following formulae,

$$(\tau'_{xz}\,,\,\tau'_{yz}) \,=\, \frac{1}{p_z\,S}\;(\tau_{xz}\,,\,\tau_{yz})\,,\;\; \sigma'_{zz} \,=\, \frac{1}{p_z}\,\sigma_{zz}\,,$$

where the S is the laminate length to thickness ratio $S = a/H$.

The discrete model is generated using a simple linear solid-shell element developed by Vu-Quoc and Tan [15, 16]. This element possesses good coarse mesh and distortion insensitivity properties for a large range of aspect ratios. Unless differently stated, the in-plane mesh consists of 14×14 elements. The minimum required number of elements in the thickness direction is three. While this is sufficient for accurate interlaminar stresses, it doesn't allow the detailed evaluation of their through the thickness variation. In the case under consideration the values of transverse stresses in the middle of every layer are also reported and, as a consequence, three more mathematical interfaces are required in these locations to give a total number of six elements through the thickness. Laminates of length to thickness ratios $S = 20, 50, 100$ are analysed and the results calculated at several points of interest are reported in table 1. Compared to Pagano's exact solutions, excellent agreement is obtained for all the considered cases.

A laminate of length to thickness ratio $S = 100$ is considered in detail to demonstrate the efficacy of the method for thin laminates. The convergence of the interlaminar stresses τ'_{xz} and σ'_{zz} at the $[0°/90°]$ interface is plotted in figure 2. Excellent agreement with Pagano's exact solution and fast convergence are obtained. The percentage error at points of maximum values compared to the exact solution is within 0.2%. Smooth distributions of interlaminar stress are observed as shown in figure 3. The same laminate has been analysed in the work of Dakshina-Moorthy and Reddy [31]. Regarding the structural symmetry, only a quarter of the plate is taken into account. An in-plane mesh of $[8 \times 8]$ nine-node quadratic elements and a mesh of linear Lagrange elements through the thickness of the laminate is considered. The interlaminar stresses are calculated and compared using three different approaches: (1) their equilibrium based stress recovery procedure, at nodes; (2) from constitutive relations, at integration points; and (3) variationally optimal stress recovery procedure, at integration points. As shown in figure 4, all the aforementioned procedures generate severe oscillations. Smoothing techniques are required. Comparing these distributions

with the ones obtained using the present procedure it can be stated that the present procedure is able to circumvent the shortcomings of the recovery procedures developed by Dakshina-Moorthy and Reddy.

A laminate of length to thickness ratio $S = 50$ is also considered to demonstrate the accuracy of the proposed procedure in analyzing moderately thick plates. Through-thickness distributions of interlaminar stresses produced using the proposed method, labelled as Equilibrium, are compared with Pagano's exact solution in figure 5 at points of major interest. Excellent agreement and fast convergence are again achieved.

Through-thickness distributions obtained using ABAQUS 6.8$^{\text{TM}}$ are also reported for comparison. The adopted elements are respectively, the 8-node linear brick incompatible modes $C3D8I$, the 20-node quadratic brick $C3D20R$, and the linear 8-node $C3D8R$. Depending on the element formulation, stresses are recovered at integration points using constructive models derived from either variational principles or other energy laws [33]. Stresses are extrapolated at nodes successively using the shape functions. Both the linear $C3D8R$ and $C3D8I$ elements do not provide single valued results at the interfaces. A through-the-thickness refinement of the mesh is required. The quadratic $C3D20R$ element does not produce an accurate estimation of the transverse shear stress τ'_{yz}. The percentage error at the point of maximum value, i.e. $z = 0$, compared to the exact solution is 9.46%.

The aforementioned results are obtained adopting one additional mathematical interface in the middle of every ply. However, these mathematical interfaces are not required to have appropriate interlaminar stress distributions using the present procedure. Figure 6 shows surface plots of the interlaminar shear stress τ'_{xz} at the $[0°/90°]$ interface obtained respectively without and with additional mathematical interfaces. An almost identical response is generated, accuracy and smoothness are satisfied regardless of the introduction of additional mathematical interfaces, implying that convergence is only related to the in-plane mesh. The present procedure uses a model with 5400 degrees of freedom and attains converged interlaminar stress results, whereas the ABAQUS's model using quadratic elements has 17595 degrees of freedom and still fails to converge.

3.2. Stress analyses of laminated composite plates with open hole subjected to uniaxial tension

Stress concentration phenomena play an important role in the design of layered structures. A well known stress concentration problem is the problem of a plate loaded in-plane and containing a circular open hole. This problem combines strong in-plane stress gradients with free edge effects and is characterized by the occurrence of strongly three-dimensional singular stress fields at the free edges in the interface between two layers of composite laminates. As a consequence, stress calculation at the interlaminar surfaces in the vicinity of the hole edge is a difficult problem.
The accuracy of the present recovery procedure is tested examining a square $[45°/-45°]_s$ plate with a circular hole as shown in figure 7. This problem has been analysed by Iarve and Pagano [34] using a method developed for the superposition of a hybrid and displacement approximation. They use asymptotic analyses to derive the hybrid stress functions and the displacement approximation is based on the polynomial B-spline functions. The laminate consist of the planar dimensions $a = 508\,mm$, diameter of the hole $D = 50.8\,mm$, coordinate of the hole center $x_c = y_c = a/2$, ply thickness $h = 2.54\,mm$. Each ply is treated as an homogeneous, elastic and orthotropic material with the following properties: $E_{11} = 138\,GPa$, $E_{22} = E_{33} = 14.5\,GPa$, $G_{12} = G_{13} = G_{23} = 5.86\,GPa$, and $\nu_{12} = \nu_{13} = \nu_{23} = 0.21$. The uniaxial loading $u_0/a = 0.001$ is applied via displacement boundary conditions at the lateral sides $(x = 0, a)$,

$$-u_x(0, y, z) = u_x(a, y, z) = u_0\,,\; u_y(0, y, z) = u_y(a, y, z) = 0. \tag{6}$$

The averaged applied stress is calculated as:

$$\sigma_0 = \frac{1}{aH} \int_0^a \int_0^H \sigma_{xx}(a, y, z)\, dy\, dz \tag{7}$$

where H is the complete laminate thickness.
Owing to the symmetry of loading and lay-up, only half of the total thickness of the laminate is modelled. The in-plane mesh is shown in figure 8, and different number of elements along the thickness direction are considered. The designation $[ner/rsr - net]$ indicates: "ner"is the number of elements extending in a radial direction from the hole edge to the end of the circular region,

$r = 80\,mm$, "rsr"is the radial spacing ratio of the elements in the circular region, and "net"is the number of elements through the half thickness. The number of elements around a quarter of the hole edge is 18.

Interlaminar stress distributions along the radial r coordinate at $\theta = 90°$, evaluated in a cylindrical coordinate system r, θ, z with the origin in the center of the plate, are shown in figure 9. These distributions are plotted starting from the hole edge up to one laminate thickness $r = H + D/2$, at the $45°/-45°$ interfacial surface, and compared with the stress fields provided by Iarve and Pagano (not reported) in the singular neighborhood of the ply interface and the hole edge. The present approach shows excellent agreement with Iarve and Pagano's distributions for a distance from the hole edge greater than one ply thickness. Convergence is reached using coarse meshes (mesh labelled as $24/30-2$ solves a system of 69120 linear equations), however, a mesh-dependent influence of the stress singularities is encountered within one ply-thickness from the hole edge. This influence is present in terms of oscillations that seem to be reduced introducing mathematical interface in the middle of every ply as far as the interlaminar shear stress $\tau_{\theta z}$ is concerned, and using a refined mesh close to the hole edge as far as the interlaminar normal stress σ_{zz} is concerned. These oscillations may be related to the high value of aspect ratio of the solid-shell element used for meshing this region, and probably generating some inaccuracy in presence of high gradients.

To understand how this mesh-dependent behaviour of the stress singularities effects the reliability of the present procedure close to the hole edge, a symmetric cross ply $[90°/0°]_s$ laminate similar to the previous one and subjected to an uniaxial tensile load σ_0 was also considered. This laminate has been analysed by Hu *et* al. [35] using a three-dimensional finite-element (FE) analysis based on displacement formulation employing a curved isoparametric 20-node element. The total length of the panel is 60 mm, the total width 30 mm, the hole radius R is 2.5 mm, and the ply thickness h is equal to 0.125 mm. Material properties are the same used for the $[45°/-45°]_s$ previously analysed.

Owing to the symmetry of loading, hole location and lay-up, only one-eight of the laminate is modelled. The in-plane mesh structure is the same used previously, with the addition of a coarse parte extended in the x direction since the laminate is not anymore square. Henceforward, if not

differently stated, the mesh adopted solves a system of 43200 linear equations. In their work, Hu *et* al. adopt a FE model consisting of 4000 elements and solving a system of 56000 linear equations. They provide stress distributions along radial lines away from the hole and around the hole at the $90°/0°$ interface, obtained by averaging the $90°$ and $0°$ ply values at the interface, a customary finite element practice. These distributions are obtained near but not at the hole edge because of the mathematical interlaminar stress singularity.

As far as the present procedure is concerned, the radial σ_{zz} distributions away from the hole at three angular positions $\theta = 0°$, $45°$, $90°$ are presented in figure 10(a). The σ_{zz} distributions have step gradients near the hole edge and approach to zero within a ply thickness from the hole. Due to the more refined mesh adopted compared to the one used in the $[45°/-45°]_s$ laminate, oscillations close to the hole edge are not anymore present, but smooth behaviours are generated. These distributions are in excellent agreement with the results (not reported) of Hu *et* al. [35]. Figure 10(b) shows the interlaminar normal stress distributions at the $90°/0°$ ply interface around the hole. As a mathematical interlaminar stress singularity exists at the free edge between the $90°$ and $0°$ plies, the computed stresses are presented near but not at the hole boundary. As the distance from the edge $(r - R)$ increases, the interlaminar stress σ_{zz} is rapidly decreased. When $(r - R) = 0.1R$, i.e. two-ply thickness away from the hole boundary, σ_{zz} becomes almost zero. σ_{zz} is compressive for most of the region around the hole with a small tensile region near $\theta = 90°$. The largest compressive σ_{zz} occurs at about $60°$ from the loading axis. The distribution obtained by Hu *et* al. at $(r - R)/R = 0.0001$ is also plotted for comparison. The maximum difference between the two distributions is within 3% at $\theta = 60°$.

The radial variation of $\tau_{\theta z}$ at $\theta = 10°$, $45°$, $75°$ is shown in figure 11(a). The decay ratio to zero varies with θ; the maximum decay ratio is at $\theta = 75°$ and, as pointed out in the plot, oscillations are still present really close to the hole edge for all the distributions. Nevertheless, these distributions are in very good agreement with the ones obtained by Hu *et* al. The circumferential interlaminar shear stress distributions $\tau_{\theta z}$ at various distances, $(r - R)/R$, from the hole boundary are shown in figure 11(b). Similar to the normal stress, σ_{zz}, the interlaminar shear stress $\tau_{\theta z}$ decreases as the distance (r-R) from the hole boundary increases and becomes small within two-ply thickness

$(0.25mm)$ from the hole. The maximum value is obtained at approximately $\theta = 75°$ from the loading axes and is $1.75\sigma_0$ which is about seven times as large as the largest σ_{zz} value computed for the same distance $r/R = 0.000082$ from the hole. This comparison indicates that, in this case, the interlaminar shear stress $\tau_{\theta z}$ is mainly responsible for the onset of delamination in the laminate. The distribution obtained by Hu *et* al. at $(r - R)/R = 0.0001$ is also plotted for comparison. The maximum difference between the two distributions is within 4% at $\theta = 75°$. The shear stress component τ_{rz} is very small compared to $\tau_{\theta z}$ and can be neglected.

The minimum distance $r/R = 0.000082$ from the hole to report the circumferential interlaminar stress distributions was selected based on two considerations. Firstly, there is a limit in the refinement of the mesh close to the hole edge since the aspect ratio of the solid element used can be increased until a certain threshold. Secondly, stress oscillations begin after the considered point and a certain error in the distributions can be introduced. To verify if these oscillations effect the prediction of delamination initiation, a stress failure criteria needs to be selected.

From the literature [36] it can be seen that the approach for predicting failure in such laminates has been that of averaging the interlaminar stresses over a distance from the hole edge, suggesting that the exact values of the stresses at the free edge are not too important. As failure stress criterion was assumed the Tsai-Wu criterion [37] which takes into account the interaction of all six stress components in a quadratic equation. Since it is assumed that the delamination initiation is mainly attributed to interlaminar stress effects, only the interlaminar stresses are considered. Moreover, since the interlaminar shear stress τ_{rz} can be neglected compared to $\tau_{\theta z}$, the Tsai-Wu criterion in a cylindrical coordinate system can be simplified as,

$$\left(\frac{\sigma_{zz}}{Z}\right)^2 + \left(\frac{\tau_{\theta z}}{S}\right)^2 = e^2 \begin{cases} e < 1 \text{ no failure} \\ e > 1 \text{ failure} \end{cases} \tag{8}$$

where Z is the interlaminar normal strength and S is the interlaminar shear strength. For positive interlaminar normal stress σ_z the uniaxial tensile strength Z_t should be used while for negative σ_z the compressive strength Z_c should be employed.

The average stress failure criteria assumes that delamination initiates when the stresses at a char-

acteristic distance a_0 from the discontinuity meet the failure criteria (8). The average of a stress component is defined as,

$$\overline{\sigma_{ij}} = \frac{1}{a_0} \int_R^{R+a_0} \sigma_{ij}\, dr \tag{9}$$

The following strength properties, $Z_t = 50.6MPa$, $Z_c = 200MPa$ and $S = 103MPa$, were used for the carbon fiber-epoxy laminates. Figure 12 shows the distributions of the e-index around the hole obtained assuming different values of a_0. The maximum value of e varies with a_0 and occurs in the region $\theta = 67.5° - 75°$ to the loading direction, indicating that these are the critical locations for delamination growth. e-indexes distributions obtained by Hu *et* al. are also reported for comparison. Slightly different values of the failure index e are obtained assuming $a_0 = 0.0005$ between 70° and 80°, but the percentage difference is always within 3%. Consequently, the oscillations of the interlaminar shear stress $\tau_{\theta z}$ close to the hole edge do not seems to influence the failure index distribution. The introduction of mathematical interfaces in the middle of every layer produces negligible variations on the results, indicating that convergence is already reached.

It is worth mentioning that the characteristic distance a_0 is experimentally determined and can vary with lay-up and hole size. Average stress failure criteria are appropriate for predicting onset of delamination but they are not suitable for failure analysis of composites, properly analysed using fracture mechanics based methods instead [38, 39].

4. Conclusion

An efficient interlaminar stress recovery procedure for three-dimensional finite elements formulations is presented. This procedure, based on equilibrium considerations, retrieves interlaminar stress values directly at the interfacial nodes between the plies and stress continuity at the inter-element boundary is automatically satisfied. As a consequence, smooth distributions are easily generated. Plates of various geometries were considered and the results were compared with available exact and Finite Element solutions. These comparisons indicated that excellent agreement was obtained with exact solutions and convergence was reached using considerably less degrees of freedom compared to other finite elements procedures. Consequently, the procedure is more suitable for design purposes. Special emphasis is placed on the problem of loaded plate with an

open circular hole. The present procedure is able to produce converged mesh-independent average interlaminar stresses even though some oscillations are encountered close to the hole edge. As such it can be effectively combined with average failure stress criteria for the prediction of delamination initiation in presence of curved free edges and stress concentrations. The present procedure is currently being implemented in the commercial Finite Element software ABAQUS 6.8^{TM}.

Acknowledgments

The useful collaboration of Prof. D.J.Rixen (Delft University of Technology, Department of Mechanical,Maritime and Materials Engineering) in the implementation of the Finite Element Tearing and Interconnecting method, is gratefully acknowledged.

References

[1] J. N. Reddy, A review of literature on finite element modelling of laminated plates., Shocks and Vibration Digest 17 (4) (1985) 3–8.

[2] T. Kant, K. Swaminathan, Estimation of transverse/interlaminar stresses in laminated composites - a selective review and survey of current developments, Composite Structures 49 (1) (2000) 65–75.

[3] J. Reddy, An evaluation of equivalent-single-layer and layerwise theories of composite laminates, Composite Structures 25 (1-4) (1993) 21–35.

[4] E. Carrera, Theories and finite elements for multilayered anisotropic, composite plates and shells, Arch. Comput. Meth. Engng 9 (2) (2004) 87–140.

[5] E. Carrera, Theories and finite elements for multilayered plates and shells: A unified compact formulation with numerical assessment and benchmarking, Archives of Computational Methods in Engineering 10 (3) (2003) 215–296.

[6] K. Washizu, Variational methods in elasticity and plasticity, 2nd edition, Pergamon Press.

[7] C. A. Felippa, On the original publication of the general canonical functional of linear elasticity, J. Appl. Mech 67 (1) (2000) 217–219.

[8] A. Mota, J. F. Abel, On mixed finite element formulations and stress recovery techniques, International Journal for Numerical Methods in Engineering 47 (1-3) (2000) 191–204.

[9] E. Carrera, Evaluation of layer-wise mixed theories for laminated plates analysis, AIAA J. 36 (5) (1998) 830–839.

[10] E. Reissner, On a certain mixed variational theorem and a proposed application, International Journal for Numerical Methods in Engineering 20 (7) (1984) 1366–1368.

[11] E. Reissner, On a mixed variational theorem and on a shear deformable plate theory, International Journal for Numerical Methods in Engineering 23 (1986) 193–198.

[12] E. Carrera, L. Demasi, Classical and advanced multilayered plate elements based upon pvd and rmvt. part 1: Derivation of finite element matrices, International Journal for Numerical Methods in Engineering 55 (2) (2002) 191–231.

[13] E. Carrera, L. Demasi, Classical and advanced multilayered plate elements based upon pvd and rmvt. part 2: Numerical implementations, International Journal for Numerical Methods in Engineering 55 (3) (2002) 253–291.

[14] J. C. Simo, M. S. Rifai, A class of mixed assumed strain methods and the method of incompatible modes, International Journal for Numerical Methods in Engineering 29 (8) (1990) 1595–1638.

[15] L. Vu-Quoc, X. G. Tan, Optimal solid shells for non-linear analyses of multilayer composites. i. statics, Computer Methods in Applied Mechanics and Engineering 192 (9-10) (2003) 975–1016.

[16] L. Vu-Quoc, X. G. Tan, Optimal solid shells for non-linear analyses of multilayer composites. ii. dynamics, Computer Methods in Applied Mechanics and Engineering 192 (9-10) (2003) 1017–1059.

[17] J. Barlow, Optimal stress locations in finite element models, International Journal for Numerical Methods in Engineering 10 (2) (1976) 243–251, 10.1002/nme.1620100202.

[18] J. T. Oden, H. J. Brauchli, On the calculation of consistent stress distributions in finite element approximations, International Journal for Numerical Methods in Engineering 3 (3) (1971) 317–325.

[19] J. S. Hinton, E. Campbell, Local and global smoothing of discontinuous finite element functions using a least squares method, International Journal for Numerical Methods in Engineering 8 (3) (1974) 461–480, 10.1002/nme.1620080303.

[20] D. J. Chen, D. K. Shah, W. S. Chan, Interfacial stress estimation using least-square extrapolation and local stress smoothing in laminated composites, Computers and Structures 58 (1996) 765–774, doi:10.1016/0045-7949(95)00181-F.

[21] J. H. Argyris, K. J. Willam, Some considerations for the evaluation of finite element models, Nuclear Engineering and Design 28 (1) (1974) 76–96.

[22] O. C. Zienkiewicz, J. Z. Zhu, The superconvergent patch recovery and a posteriori error estimates. part 1: The recovery technique, International Journal for Numerical Methods in Engineering 33 (7) (1992) 1331–1364.

[23] O. C. Zienkiewicz, J. Z. Zhu, The superconvergent patch recovery and a posteriori error estimates. part 2: Error estimates and adaptivity, International Journal for Numerical Methods in Engineering 33 (7) (1992) 1365–1382.

[24] T. Blacker, T. Belytschko, Superconvergent patch recovery with equilibrium and conjoint interpolant enhancements, International Journal for Numerical Methods in Engineering 37 (3) (1994) 517–536.

[25] N. E. Wiberg, F. Abdulwahab, S. Ziukas, Enhanced superconvergent patch recovery incorporating equilibrium and boundary conditions, International Journal for Numerical Methods in Engineering 37 (20) (1994) 3417–3440.

[26] T. Lee, H. Park, S. Lee, A super-convergent stress recovery technique with equilibrium constraint, International Journal for Numerical Methods in Engineering 40 (6) (1997) 1139–1160.

[27] J. Yuan, A. Saleeb, A. Gendy, Stress projection, layerwise-equivalent formulation for accurate predictions of transverse stresses in laminated plates and shells, International J. Computational Engineering Science 1 (1) (1982) 91–138.

[28] G. Prathap, B. P. Naganarayana, Consistent force resultant distributions in displacement elements with varying sectional properties, International Journal for Numerical Methods in Engineering 29 (4) (1990) 775–783.

[29] G. Prathap, B. P. Naganarayana, Consistent thermal stress evaluation in finite elements, Computers and Structures 54 (3) (1995) 415–426.

[30] S. de Miranda, F. Ubertini, Recovery of consistent stresses for compatible finite elements, Computer Methods in Applied Mechanics and Engineering 191 (15-16) (2002) 1595–1609.

[31] C. M. Dakshina Moorthy, J. N. Reddy, Recovery of interlaminar stresses and strain energy release rates in composite laminates, Finite Elements in Analysis and Design 33 (1) (1999) 1–27.

[32] N. J. Pagano, Exact solutions for rectangular bidirectional composites and sandwich plates, Journal of Composite Materials 4 (1) (1970) 20–34.

[33] Abaqus analysis user's manual-abaqus version 6.8.

[34] E. V. Iarve, N. J. Pagano, Singular full-field stresses in composite laminates with open holes, International Journal of Solids and Structures 38 (1) (2001) 1–28.

[35] F. Z. Hu, C. Soutis, E. C. Edge, Interlaminar stresses in composite laminates with a circular hole, Composite Structures 37 (1997) 223–232.

[36] J. C. Brewer, P. A. Lagace, Quadratic stress criterion for initiation of delamination, Journal of Composite Materials 22 (12) (1988) 1141–1155.

[37] S. W. Tsai, H. T. Hahn, Introduction to composite materials, Technomic Publishing Co.

[38] M. Kashtalyan, C. Soutis, Strain energy release rate for off-axis ply cracking in laminated composites., Int. J. Fracture 112 (2) (2001) 3–8.

[39] M. Kashtalyan, C. Soutis, Analysis of local delaminations induced by angle ply matrix cracks., Int. J. Solids and Structures 39 (6) (2002) 1515–1537.

Table 1: Recovered stress fields considering different values of length to thickness ratio S.

S		$\tau'_{xz}(-\frac{a}{2},0,0)$	$\tau'_{yz}(0,-\frac{a}{2},0)$	$\sigma'_{zz}(0,0,H/6)$
20	EXACT	0.3846	0.0938	0.7398
	EQUILIBRIUM	0.3845	0.0938	0.7429
50	EXACT	0.3934	0.0842	0.7406
	EQUILIBRIUM	0.3928	0.0841	0.7436
100	EXACT	0.3946	0.0828	0.7407
	EQUILIBRIUM	0.3926	0.0823	0.7434

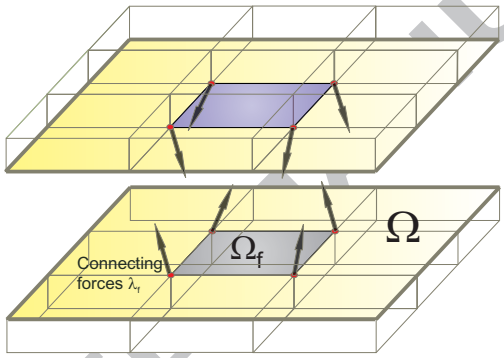

Figure 1: Connecting forces $\boldsymbol{\lambda}_f$ at the interfacial nodes of each element obtained by the FETI method

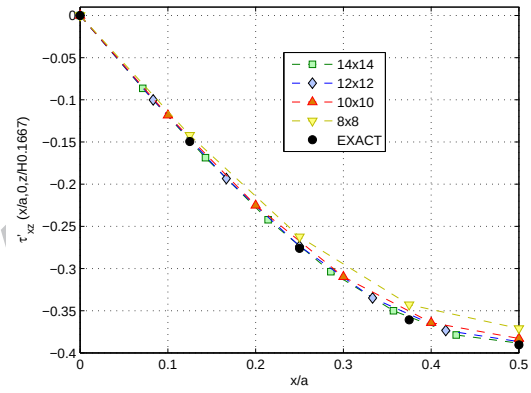

(a) Convergence of the interlaminar shear stress τ'_{xz} with different in-plane meshes.

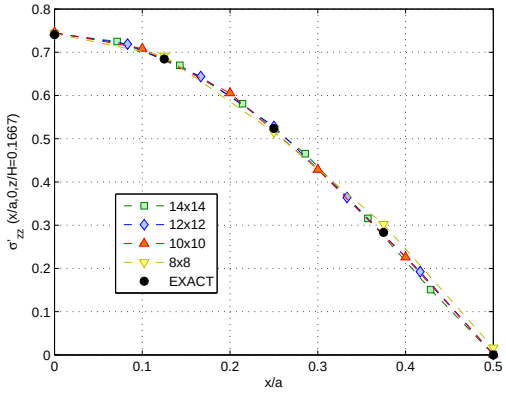

(b) Convergence of the interlaminar normal stress σ'_{zz} with different in-plane meshes.

Figure 2: Convergence of the recovered interlaminar transverse stresses at the $[0°/90°]$ interface and $y = 0$ of a $[0°/90°/0°]$ laminate, $S = 100$.

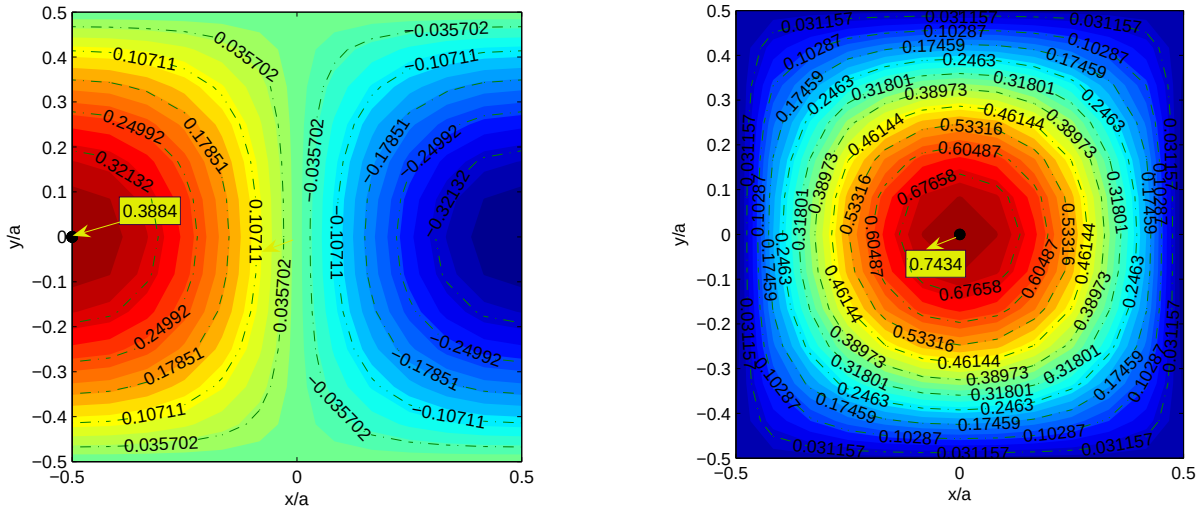

(a) Surface plot of the interlaminar shear stress τ'_{xz}.

(b) Surface plot of the interlaminar normal stress σ'_{zz}.

Figure 3: Surface plot of the recovered interlaminar stresses at the $[0°/90°]$ interface of a $[0°/90°/0°]$ laminate, $S = 100$.

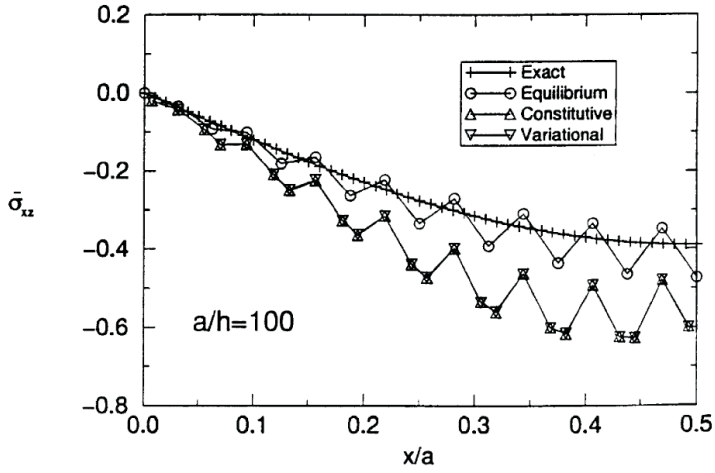

Figure 4: Shear stress distribution τ'_{xz} at the interlaminar surface $[0°/90°]$ and $y = 0$ of a $[0°/90°/0°]$ laminate obtained by Reddy and Dakshina-Moorthy [31] considering different approaches, $S = 100$.

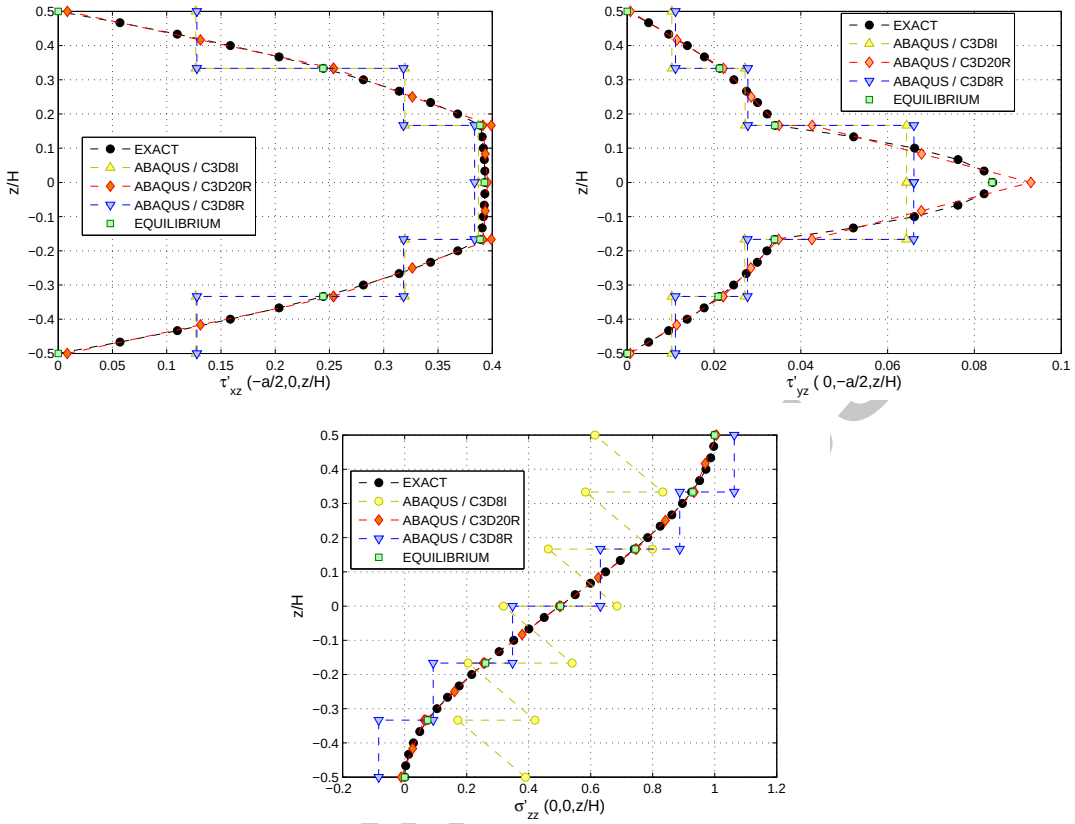

Figure 5: Comparisons between through-thickness distributions of the transverse stresses obtained using the present equilibrium based procedure, using different ABAQUS's elements, and Pagano's exact solution, $S = 50$.

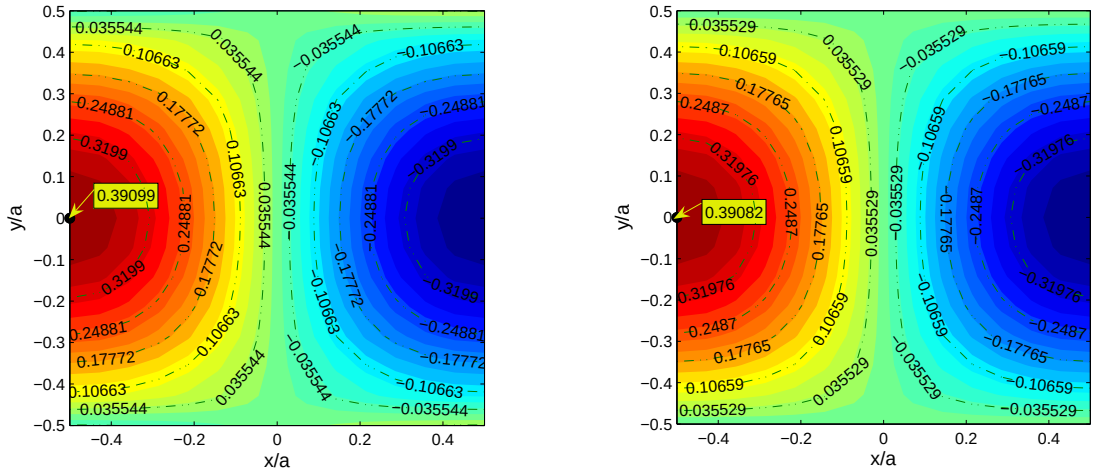

(a) Surface plot of the interlaminar shear stress τ'_{xz} obtained without additional mathematical interfaces.

(b) Surface plot of the interlaminar shear stress τ'_{xz} obtained with one additional mathematical interfaces for every layer.

Figure 6: Surface plot of the recovered interlaminar shear stress τ'_{xz} at the $[0°/90°]$ interface of a $[0°/90°/0°]$ laminate, $S = 50$.

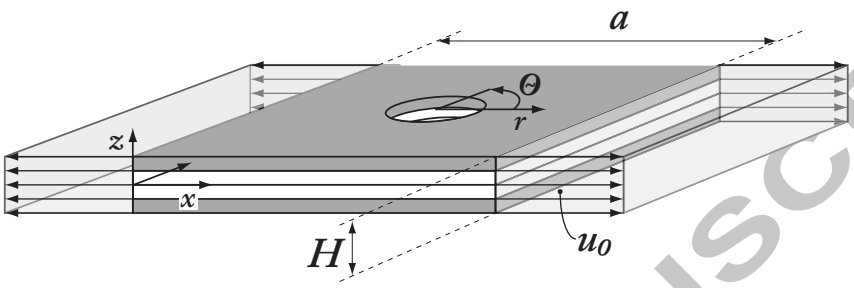

Figure 7: Laminate plate with hole.

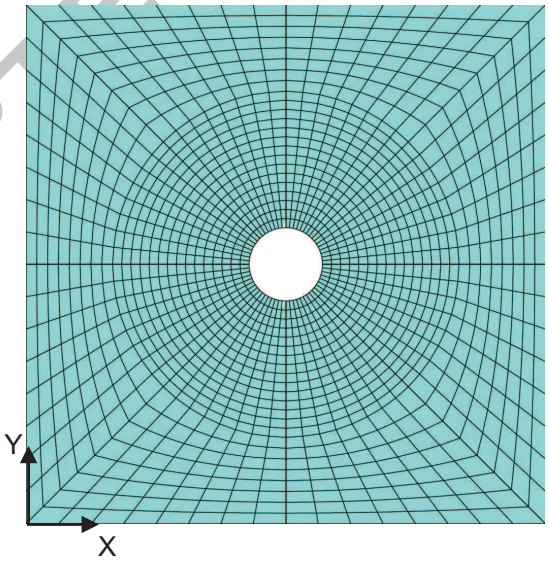

Figure 8: Example of the adopted mesh

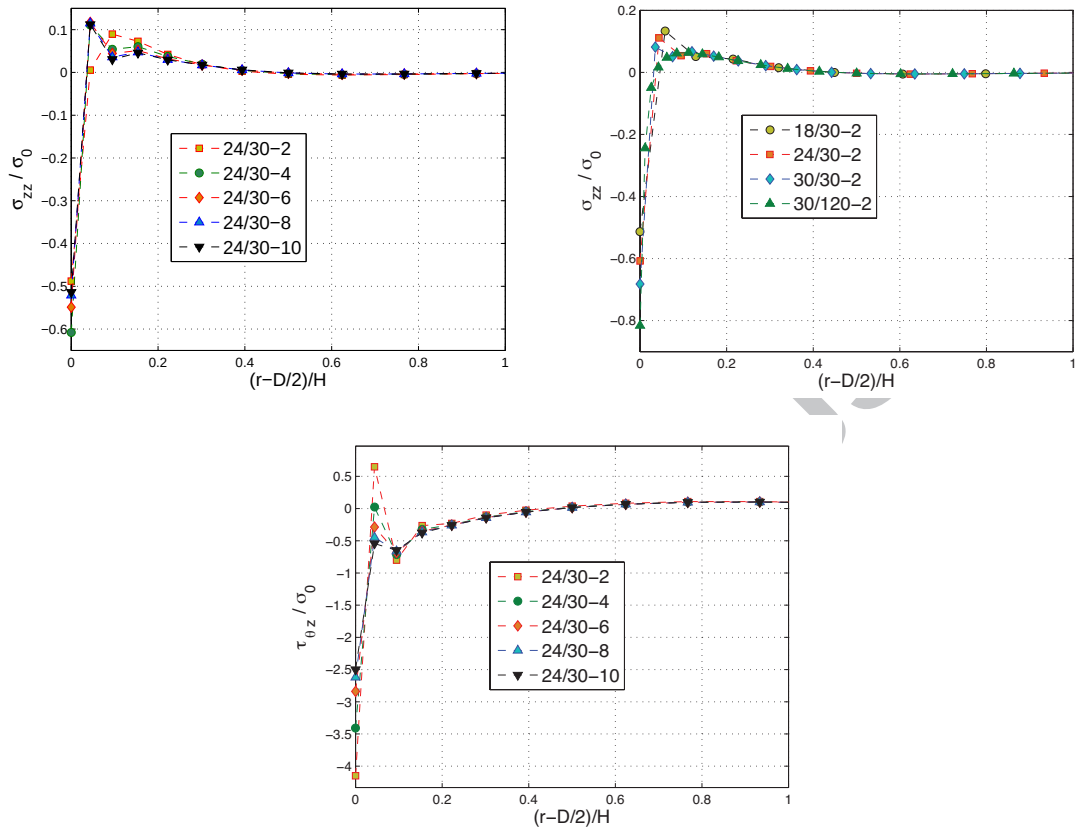

Figure 9: Interlaminar transverse stress distributions at the $45°/-45°$ interface of a $[45°/-45°]_s$ symmetric laminate, $\theta = 90°$, from the hole edge up to one laminate thickness with different meshes.

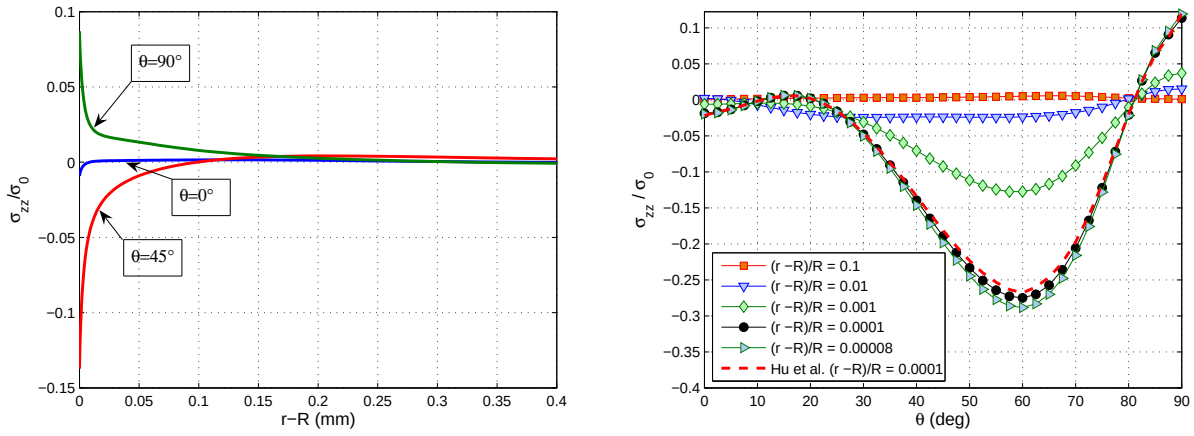

(a) Normalized interlaminar normal stress distributions in the radial directions $\theta = 0°, 45°$ and $90°$.

(b) Normalized interlaminar normal-stress distributions around the hole.

Figure 10: Normalized interlaminar normal stress distributions σ_{zz}/σ_0 at the $90°/0°$ interface of a $[90°/0°]_s$ symmetric laminate.

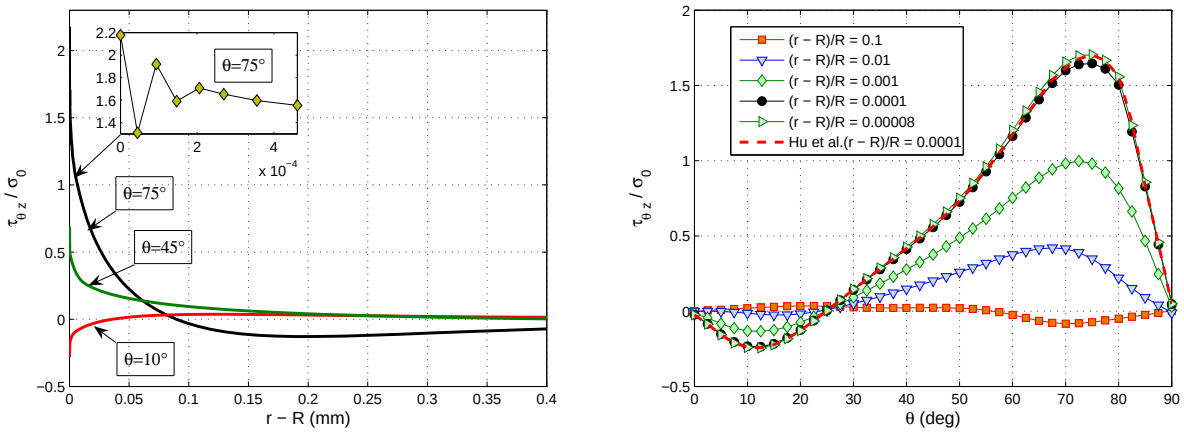

(a) Normalized interlaminar shear stress distributions at different angular positions.

(b) Normalized interlaminar shear stress distributions around the hole.

Figure 11: Normalized interlaminar shear stress distributions $\tau_{\theta z}/\sigma_0$ at the $90^\circ/0^\circ$ interface of a $[90^\circ/0^\circ]_s$ symmetric laminate.

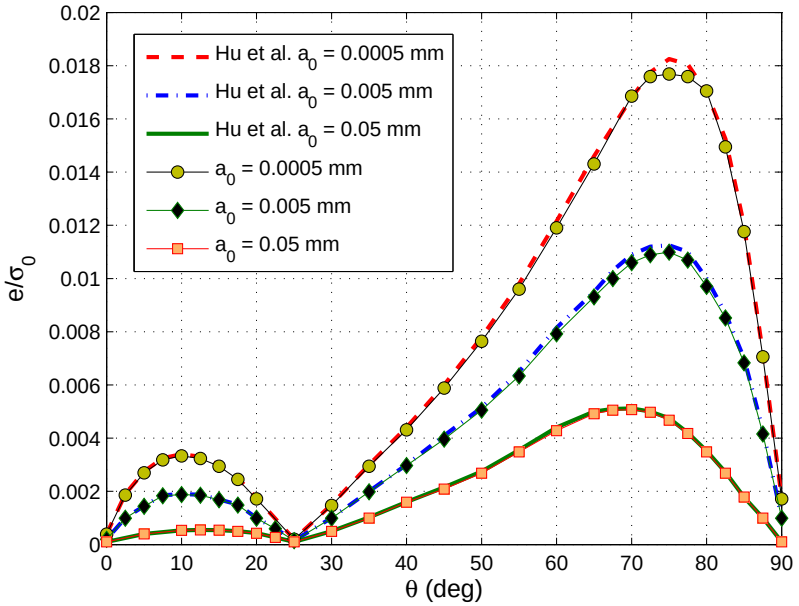

Figure 12: e-index distributions at the $90^\circ/0^\circ$ interface of a $[90^\circ/0^\circ]_s$ symmetric laminate near the hole edge determined by the average stress criterion.